Simultaneous optical trapping and detection of atoms by microdisk resonators

Michael Rosenblit,[1] Yonathan Japha,[1] Peter Horak,[2] and Ron Folman[1]
[1]*Department of Physics and Ilse Katz Center for Meso- and Nanoscale Science and Technology, Ben Gurion University of the Negev, P.O. Box 653, Be'er Sheva 84105, Israel*
[2]*Optoelectronics Research Centre, University of Southampton, Southampton SO17 1BJ, United Kingdom*
(Received 23 January 2006; published 6 June 2006)

We propose a scheme for simultaneously trapping and detecting single atoms near the surface of a substrate using whispering gallery modes of a microdisk resonator. For efficient atom-mode coupling, the atom should be placed within approximately 150 nm from the disk. We show that a combination of red and blue detuned modes can form an optical trap at such distances while the backaction of the atom on the field modes can simultaneously be used for atom detection. We investigate these trapping potentials including van-der-Waals and Casimir-Polder forces and discuss corresponding atom detection efficiencies, depending on a variety of system parameters. Finally, we analyze the feasibility of nondestructive detection.

DOI: 10.1103/PhysRevA.73.063805 PACS number(s): 42.50.Ct, 42.82.−m, 32.80.Qk

I. INTRODUCTION

Optical microresonators are currently attracting a lot of interest in a variety of fields ranging from telecommunication [1] to biological/chemical sensors [2]. In particular, the advancement of microdisk resonators may lead to the development of compact and integrable optical-electronic devices. Recently, significant progress in increasing the finesse of such resonators has been reported [3], which makes these devices interesting for future applications in the emerging field of quantum technology [4–8].

Combining high-Q microresonators with miniaturized magnetic traps for cold, neutral atoms above a substrate, so-called atom chips [9], may lead to integrated devices that allow for a high degree of control over light-atom interaction. Such systems may have a significant impact in contexts such as cavity quantum electrodynamics (QED) [10], single photon sources [4], memory and purifiers for quantum communication [5], manipulation of matter waves in interferometric sensors [6], atomic clocks [7], and the quantum computer [5,8]. Such an integrated photonics device for quantum technology would not only improve technical capabilities such as enhanced robustness and accuracy while reducing size, cost, and power consumption, it may also give rise to complex new functionalities such as nondestructive atom-light interaction and high signal-to-noise detection, high-fidelity qubit transfer and entanglement for quantum communication, and scalability for, e.g., the quantum computer.

Several different realizations of microresonators are currently under investigation in the context of their integration on atom chips, e.g., Fabry-Perot fiber cavities [11], photonic band-gap structures [12], and microdisk resonators [13]. The latter possibility is attractive since it combines the high optical quality of the much studied microsphere [14–16] with advanced microfabrication and integration technology.

In this paper, we follow up on our recent proposal of using the whispering gallery modes (WGM) of a toroid microcavity for single-atom detection [13] with a detailed analysis of the effects of detection on the atomic external degrees of freedom. In particular, we show that the same optical modes that are used for atom detection can be exploited to create a trapping potential for the atom. The parameters can be adjusted to provide a sufficiently deep potential minimum at an appropriate distance from the disk surface to hold the atom securely in place during the detection process.

This work is organized as follows. First, we review the system under consideration and the principles of optical single-atom detection in such a device in Sec. II. Next, in Sec. III, we discuss the different optical, magnetic, and surface forces and potentials operating on the atom. In Sec. IV, we investigate a trapping scheme that simultaneously allows for optical atom detection. In Sec. V, we present results on an optimized set of parameters for simultaneous trapping and detection and discuss the performance of the detector and the dynamics of the atom during the detection. Finally, we discuss the experimental feasibility and conclude in Sec. VI.

II. SYSTEM DESIGN AND OPERATION SCHEME

A. System design

The basic system under consideration and its optical properties have been discussed in detail elsewhere [13]. Here we will only give a brief summary.

We consider an atom chip consisting of a magnetic trap for cold atoms and an optical resonator for atom trapping and detection as shown in Fig. 1.

The optical resonator is a microdisk or a toroid made of a dielectric material [3], which supports high-finesse whispering gallery modes near the wavelengths of the $D1$ and $D2$ lines of rubidium atoms, i.e., around 795 and 780 nm, respectively. Light is coupled into and out of the cavity through evanescent-field coupling across an air gap by a tapered linear waveguide that is mode-matched to achieve best coupling.

Atoms are initially loaded into a magnetic trap [17] formed by a Z-shaped current-carrying wire, as shown in Fig. 1, with its center located at about 50–250 nm from the side wall of the disk. Typically the wire has a rectangular shape with width and height of 1 μm, embedded 0.5 μm below the surface of the chip. Assuming wire currents of

 ©2006 The American Physical Society

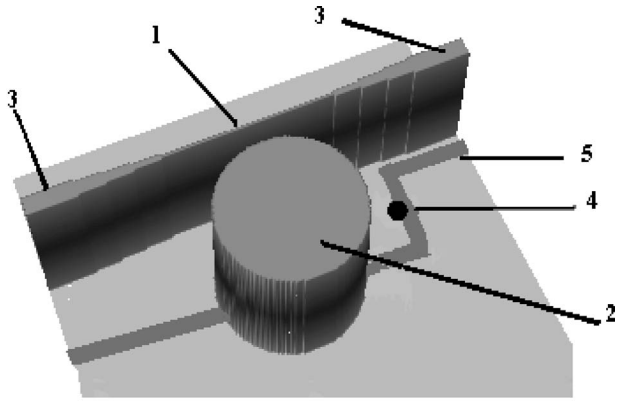

FIG. 1. The structure under consideration. The evanescent wave from the slab waveguide (1) is coupled into the disk (2) and back through a small gap between them. The adiabatic waveguide tapers (3) serve for coupling light from optical fibers (not shown) into and out of the waveguide. Cold atoms (4) can be brought to the disk side via the magnetic field of a Z-shaped current-carrying wire (5) [9]. However, as explained in this work, such a magnetic trap is not suitable to hold the atoms during detection, and so other means of trapping are described for this operation.

~100 mA and a homogeneous bias field of 100 G, a magnetic trap is formed approximately 2 μm above the surface. However, as will be discussed later, the magnetic trap is in general too weak to provide atom confinement during the optical detection process. The atoms are therefore transferred into an optical trap formed by the evanescent waves of two microdisk modes of opposite detuning. The atom-light coupling also changes the optical properties of the disk modes, which can subsequently be measured in order to infer the presence of the atom.

The results presented in this work are based on a semianalytic coupled mode theory [18,19] of the optical properties of the system and a standard Jaynes-Cummings type model of the atom-light interaction.

B. Single-atom detection

As was described in detail in [13], our detection scheme works as follows. Light that is resonant with one microdisk mode is coupled into the linear waveguide from one side. The output field at the other end of the waveguide is mixed with a strong local oscillator field in a balanced detector. The presence of the atom is then inferred from a change in the intensity difference between the two arms of the balanced detector.

We have shown previously that, in the limit of far detuning of the light field from the atomic transition and for low atomic saturation, the signal-to-noise ratio of this atom detection scheme is given by

$$S = 4\sqrt{\tau}|A_{\mathrm{in}}|\frac{\kappa_T g^2}{\Delta \kappa^2}, \tag{1}$$

where τ is the measurement time, A_{in} is the amplitude of the pump light in the linear waveguide normalized such that $|A_{\mathrm{in}}|^2$ is the power in units of photons per second, κ_T is the cavity decay rate due to microdisk-waveguide coupling, κ is the total cavity decay rate including losses, Δ is the atom-light detuning, and g is the single-photon Rabi frequency. The corresponding photon number in the cavity is given by

$$N = 2|A_{\mathrm{in}}|^2\frac{\kappa_T}{\kappa^2}. \tag{2}$$

The optical properties of selected WGMs near resonance with either the $D1$ or $D2$ transition lines of ^{87}Rb (at 795 and 780 nm, respectively) are summarized in Table I for disk diameters 15 and 30 μm. $Q_1(Q_2)$ is the total quality factor defined by $Q=\omega/(2\kappa)$ [13]. As discussed below (Sec. IV), only modes that are blue-detuned with respect to the $D2$ line and red-detuned with respect to the $D1$ line are eventually proposed for detection and trapping. We assume a root-mean-square surface roughness of $\sigma=1$ nm and a surface correlation length of $L_c=5$ nm throughout this paper [13].

Let us now derive an estimate for the light field intensity required for single-atom detection. Assume we want to detect a Rb atom using the interaction of the $D2$ line (780 nm wavelength) with the $(l=167, q=1)$ mode of a 30-μm-diam disk, see Table I for details. The atom is assumed to be located 100 nm off the surface of the disk for a time $\tau=10$ μs. In order to detect the atom with a signal-to-noise ratio of $S=10$, the required input power is $|A_{\mathrm{in}}|^2 \approx 0.12 \times 10^{14}$ photons per second (3 μW). The corresponding number of photons in the cavity is $N \approx 2.4 \times 10^5$ for a gap size of 0.6 μm.

TABLE I. Optical properties of selected WGMs. Q_1 (Q_2) is the quality factor for a waveguide-disk gap size of 0.5 μm (0.9 μm), l is the longitudinal mode index (the radial index is $q=1$), g_0 is the single-photon Rabi frequency for an atom at the disk boundary, and α is the decay constant of the evanescent field.

D (μm)	l	λ (nm)	Q_1 (units of 10^6)	Q_2 (units of 10^8)	g_0 (MHz)	α ($1/\mu$m)
30	168	774.2	3.2	1.49	100.5	7.49
30	167	778.73	3.0	1.47	102.6	7.7
30	166	783.27	2.79	1.46	103.2	7.19
30	163	797.2	2.27	1.39	105.0	7.3
15	82	771.3	1.56	0.77	202.5	7.06
15	79	799.2	1.02	0.70	209.8	6.75

III. FORCES AND POTENTIALS

In this section, we describe the forces on an atom situated near the surface of the microdisk: optical forces due to the interaction with the light fields near the disk, van der Waals forces due to the interaction with the dielectric surface, and optionally magnetic forces generated by current-carrying metal wires on the surface of the chip. In general, the combined effect of these interactions is quite complex. In order to simplify the discussion, we will assume in the following the limit of low atomic saturation, where the combined potential is a simple sum of the various contributions,

$$V = V_{\text{light}} + V_{\text{AS}} + V_{\text{mag}}. \tag{3}$$

Here V_{light} is the optical potential, V_{AS} is the atom-surface potential, and V_{mag} is the magnetic potential of the wire trap.

A. Atom-light interaction

In this section, we will assume fixed light intensities in the cavity and only discuss the effects of the light on the atom. The Hamiltonian of the interaction of a single atom with several optical modes in the dipole and rotating-wave approximations is given by

$$H_{\text{light}} = \frac{i\hbar}{2}\sum_j \sum_{m>n} [\Omega_{j,mn}(\mathbf{x})e^{i\omega_j t}|m\rangle\langle n| - \Omega^*_{j,mn}(\mathbf{x})e^{-i\omega_j t}|n\rangle\langle m|]. \tag{4}$$

Here $|m\rangle$ and $|n\rangle$ are different atomic electronic levels and $\Omega_{j,mn}$ is the interaction amplitude between the disk mode j with frequency ω_j and the atom transition $|n\rangle \rightarrow |m\rangle$, such that level $|m\rangle$ has a higher energy than $|n\rangle$. Note that different modes may be frequency-degenerate (e.g., two counterpropagating modes) and may couple to the same atomic transition. In the following, we assume coherent states for the cavity modes and therefore [13]

$$\Omega_{j,mn}(\mathbf{x}) = 2g_j(\mathbf{x})\sqrt{N_j}, \tag{5}$$

where N_j is the number of cavity photons and $g_j(\mathbf{x})$ is the single-photon Rabi frequency of mode j for the relevant transition in an atom at position $\mathbf{x}$ in the evanescent field of the disk mode. The maximum values of g_j at the disk surface for several selected modes and the decay constants of their evanescent fields are given in Table I.

In the simple case of a light field with a single frequency ω, the Bloch equations for the density matrix of the two-level atom (with ground state $|0\rangle$ and excited state $|1\rangle$) fixed at a given point $\mathbf{x}$ have the steady-state solution

$$\rho_{11}(\mathbf{x},t) = \frac{1}{2}\frac{|\Omega(\mathbf{x})|^2}{|\Omega(\mathbf{x})|^2 + 2\Delta^2 + 2\Gamma^2}, \tag{6}$$

$$\rho_{01}(\mathbf{x},t) = -\frac{\Omega(\mathbf{x})(\Gamma - i\Delta)}{|\Omega(\mathbf{x})|^2 + 2\Delta^2 + 2\Gamma^2}e^{-i\omega t}, \tag{7}$$

where 2Γ is the decay rate of the excited-state population by spontaneous emission and $\Delta = \omega - \omega_{01}$ is the detuning of the mode frequency from the atomic transition frequency. The light force on the atom is given by

$$\mathbf{F} = -\text{Tr}\{\rho(\mathbf{x})\,\boldsymbol{\nabla} H_{\text{light}}\}. \tag{8}$$

If the atomic motion is slow enough such that the change in the light intensity at the atomic location is small during the decay time $1/(2\Gamma)$, an adiabatic atomic potential may be defined that is the spatial integral of the force (8) using the steady-state density matrix (6), (7). This yields

$$V_{\text{light}} = \frac{\hbar\Delta}{2}\log\left[1 + \frac{\Omega^2}{2\Gamma^2 + 2\Delta^2}\right] \approx -\frac{\hbar\Delta}{2}\log[1 - 2\rho_{11}]. \tag{9}$$

For $\Omega, \Gamma \ll \Delta$ the potential may be approximated by

$$V_{\text{light}}(\mathbf{x}) \approx \frac{\hbar|\Omega(\mathbf{x})|^2}{4\Delta}, \tag{10}$$

which is positive (repulsive) for $\Delta > 0$ ("blue-detuned" light) and negative (attractive) for $\Delta < 0$ ("red-detuned" light). Using the values of the parameter estimate of Sec. II B, we find that the force on an atom 100 nm away from the disk surface is about 70 μK/nm.

For later use in this paper, we now discuss the combined optical potential of two light fields interacting simultaneously with the atom, where one field is blue-detuned and the other is red-detuned. Two possibilities can be considered: (i) where the two fields couple the atomic ground state to two different excited states (three-level situation), or (ii) where both light fields operate on the same atomic transition (two-level situation).

In the three-level situation, e.g., when the two light fields operate on the $D1$ and $D2$ lines of rubidium, respectively, an exact analytic solution of the optical Bloch equations for the atomic density matrix can be found. In the limit of low atomic saturation, the steady-state 3×3 density matrix may be approximated by a direct product of the 2×2 matrices for the two atomic transitions independently. The optical potential is then found as the sum of two terms given by Eq. (10) corresponding to the two fields.

The situation is slightly more complicated in the two-level case. Because of interference between the two light fields oscillating at different frequencies, no steady-state solution exists in this case. Instead, the atomic density matrix, and hence the optical force and the dipole potential, oscillate with the difference frequency $|\Delta_1 - \Delta_2|$. However, in the limit of low atomic saturation it can be shown that the potential oscillates around a mean value that is the sum of the steady-state potentials expected from each of the light fields alone. Moreover, because of the large detuning envisaged here between microdisk modes and atomic transitions of the order of THz, the oscillation frequency $|\Delta_1 - \Delta_2|$ is much larger than the typical kinetic energy of the atom. Therefore, the atom will move under an effective potential that is the time average of the oscillating potential.

We therefore find that in both configurations, the two-level and the three-level situations, the optical potential can be approximated by the sum of two terms of the form (10),

$$V_{\text{light}}(\mathbf{x}) \approx V_{\text{light},1}(\mathbf{x}) + V_{\text{light},2}(\mathbf{x}) \approx \frac{\hbar|\Omega_1(\mathbf{x})|^2}{4\Delta_1} + \frac{\hbar|\Omega_2(\mathbf{x})|^2}{4\Delta_2}. \tag{11}$$

B. Atom-surface interaction

An atom near a dielectric or conducting surface experiences an effective potential due to the interaction of the atomic dipole with the dipole moments created in the material. At very short distances this potential is a van der Waals potential due to static dipole-dipole interaction, while at larger distances of the order of one wavelength of the atomic transition, the retardation effect changes the nature of the potential and it is then called the Casimir-Polder potential [20]. For a ground-state atom, the atom-surface potentials are usually attractive. The asymptotic form of the atom-surface potential at very short distances from a nonmagnetic and nondissipative dielectric material with refractive index n is

$$V_{\text{vdW}}(x) = -\left(\frac{n^2-1}{n^2+1}\right)\frac{\langle d_\parallel^2\rangle + 2\langle d_\perp^2\rangle}{8\pi\epsilon_0(2x)^3}, \tag{12}$$

where $d_\parallel, d_\perp$ are the components of the atomic dipole moments parallel and perpendicular to the surface, respectively. For an isotropic atom $\langle d_\parallel^2\rangle + 2\langle d_\perp^2\rangle = \frac{4}{3}e^2\langle r^2\rangle$, where e is the electron charge and $\langle r^2\rangle$ is the expectation value of the square of the atomic radius.

The atom-surface potential in the retarded regime, the Casimir-Polder potential, takes the form

$$V_{\text{CP}}(x) = -\frac{\hbar c}{2\pi^2\epsilon_0(2x)^4}\sum_j \frac{c_4^\parallel\langle d_\parallel^2\rangle + c_4^\perp\langle d_\perp^2\rangle}{E_{ji}}, \tag{13}$$

where E_{ji} is the energy difference between atomic levels i and j, $d_\parallel, d_\perp$ are matrix elements of the atomic dipole between the two levels at directions parallel and perpendicular to the surface, and the coefficients $c_4^\parallel, c_4^\perp$ are functions of the refractive index n (see Ref. [20]) ranging between 0 for $n=1$ and 1 for $n\to\infty$ (a perfect conductor). We assume an isotropic atomic dipole moment and use the identity

$$\alpha_0 = \sum_j \frac{|\langle j|d|i\rangle|^2}{E_{ji}}, \tag{14}$$

where α_0 is the static polarizability of the atom. We then obtain

$$V_{\text{CP}}(x) = -\frac{\alpha_0\hbar c}{2\pi^2\epsilon_0(2x)^4}(2c_4^\parallel + c_4^\perp). \tag{15}$$

The form of the van der Waals potential given by Eq. (12) is valid for very short distances (of the orders of a few nanometers), while the forms of the Casimir-Polder potential, Eqs. (13) and (15), hold for large distances (of the order of one micrometer or more). In the intermediate regime, the exact potential involves cumbersome integrals that may be performed numerically. For simplicity, we make the following approximation:

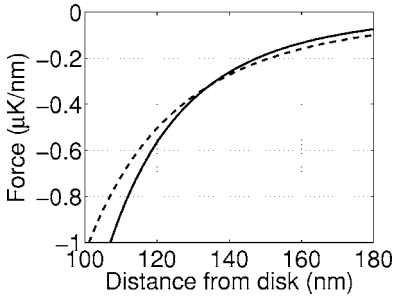

FIG. 2. Atom-surface asymptotic forms of the force vs atom distance from the microdisk: Casimir-Polder potential (solid line) and van der Waals potential (dashed line).

$$V_{\text{AS}}(x) \approx \int^x dx' \max\{F_{\text{vdW}}(x'), F_{\text{CP}}(x')\}, \tag{16}$$

where F_{vdW} and F_{CP} are the derivatives of the corresponding potentials in the radial direction. At short distances we hence approximate the atom-surface potential by V_{vdW}, while at large distances we use $V_{\text{AS}} = V_{\text{CP}}$.

Figure 2 shows the two asymptotic forms of the force (derivative of the potentials) plotted over the whole range of distances for a rubidium atom near a silica surface (refractive index $n=1.454$). The transition point between these two asymptotic forms is found at a distance of about 130 nm from the microdisk surface. The van der Waals force at the distance of 50 nm is about 3 μK/nm and at 100 nm it is about 1 μK/nm. These values are therefore much smaller than the repulsive force created by the blue-detuned detection light as estimated above.

Note that the Casimir-Polder interaction changes with temperature [21]. However, the temperature-dependent correction factor is mainly important for long atom-surface distances of the order of a few micrometers, and here we neglect these temperature effects.

C. Magnetic trap potential

The magnetic field **B** created by current-carrying wires on the chip interacts with the magnetic moment $\boldsymbol{\mu}$ of the atom through the Hamiltonian $H_{\text{mag}} = -\boldsymbol{\mu}\cdot\mathbf{B}$. A hyperfine atomic level with $F>0$ splits in the magnetic field into its Zeeman sublevels with magnetic moments following the direction of the magnetic field while moving adiabatically in the region of the field. The potential for a specific Zeeman level with quantum number m_F is

$$V_{m_F}(\mathbf{x}) = m_F g_F \mu_B |\mathbf{B}(\mathbf{x})|, \tag{17}$$

where μ_B is the Bohr magneton and g_F is the Landé factor corresponding to the hyperfine level F. Atomic levels with $m_F>0$ are attracted to the minimum of the field, the $m_F=0$ level feels no potential, and $m_F<0$ levels are repelled from the minimum of the field. A two-dimensional confinement of levels with $m_F>0$ is achieved above a straight wire with the help of an external bias field. Three-dimensional confinement is achieved by the combination of several wires or by a single wire with a U or Z shape.

A magnetic trap above an atomic chip is usually formed by a combination of magnetic-field components from three sources: (a) A wire in the y direction on the chip surface carrying a current I generates a magnetic field $\mathbf{B}\approx 2\times 10^{-3} I(z\hat{\mathbf{x}}-x\hat{\mathbf{z}})/(x^2+z^2)$ above the wire (I is in amperes, $\mathbf{B}$ in Gauss, and x, z in meters). (b) A bias field $-B_0\hat{\mathbf{x}}$ that cancels the magnetic field generated by the wire at height $z_0=2I/B_0$ from the center of the wire at $x=0$. (c) An offset field $B_{\text{offset}}\hat{\mathbf{y}}$, which prevents the magnetic field at the center of the trap from being zero. The potential near the center of the trap at $\mathbf{x}_0=(0,0,z_0)$ is then given by

$$\mathbf{B}\approx\left((z-z_0)\frac{\partial B_x(\mathbf{x}_0)}{\partial z},B_{\text{offset}},x\frac{\partial B_z(\mathbf{x}_0)}{\partial x}\right), \tag{18}$$

where $\partial B_x/\partial z=\partial B_z/\partial x\approx 2\times 10^{-3} I/z_0^2$. In the range where $(z-z_0)\,\partial B_x/\partial z$, $x\,\partial B_z/\partial x\ll B_{\text{offset}}$ the potential is approximately harmonic,

$$V_{\text{mag}}(\mathbf{x})\approx m_F g_F\mu_B\left\{B_{\text{offset}}+\frac{2I^2 10^{-3}}{z_0^4 B_{\text{offset}}}[x^2+(z-z_0)^2]\right\}, \tag{19}$$

with oscillation frequency

$$\omega_{\text{ho}}=\frac{2\times 10^{-3} I}{z_0^2}\sqrt{\frac{m_F g_F\mu_B}{mB_{\text{offset}}}}. \tag{20}$$

For a Z-shaped trap usually $B_{\text{offset}}\approx B_0\approx 10^{-3}2I/z_0$. The potential is then harmonic in the range $|x|,|z-z_0|<z_0$ and the trapping frequency becomes

$$\omega_{\text{ho}}\approx\frac{1}{z_0}\sqrt{\frac{2\times 10^{-3} I m_F g_F\mu_B}{mz_0}}. \tag{21}$$

Conventional wires can carry a current density of up to 10^7 A/cm^2. For a wire of cross section 1 μm^2, this implies a maximum current of 0.1 A. It follows that for ^{87}Rb atoms in the state $|F=2,m_F=2\rangle$, a typical harmonic-oscillator frequency of a magnetic trap can reach up to $\omega_{\text{ho}}=2\pi\times 35$ kHz at trap heights of $z_0=3$ μm above the wire center (2.5 μm above the top surface of the wire). The energy splitting between magnetic states with different m_F ($\Delta m_F=1$) is given by

$$\Delta E\sim\Delta m_F g_F\mu_B|B_{\text{offset}}|. \tag{22}$$

For the strong magnetic trap at a height of 3 μm, the energy splitting of a Z-trap is approximately 50 MHz. The maximal force that can be applied to the atom by the magnetic field is given by the magnetic potential gradient, $|F_{\text{mag}}|\approx 2\times 10^{-3}\mu_B I/z_0^2$, which is of the order of 1.5 μK/nm. This value is much smaller than the force applied by the evanescent light fields of the disk. This implies that a magnetic field by itself cannot hold the atom against the repulsive force of the detection light.

Magnetic fields may still be considered for atom trapping in the angular direction (along the perimeter of the disk) where no light forces exist. However, this option is also problematic because of light-induced Raman transitions into untrapped Zeeman levels. Raman transitions between different magnetic atomic levels occur because of stimulated photon absorption and reemission processes without significantly populating a higher electronic level of the atom. In principle, such transitions can be suppressed by controlling the polarizations of the optical fields. However, in the case of an evanescent field near the surface of a microdisk, the field polarization cannot be controlled. Raman transitions will therefore occur with an effective oscillation frequency

$$\Omega_{\text{eff}}\sim\frac{Ng(\mathbf{x})^2}{\Delta}. \tag{23}$$

If the value of Ω_{eff} between two magnetic levels is larger than the frequency splitting δ between the two levels, significant oscillations will take place between the levels with flipping times $t_{\text{flip}}=\pi/(2\Omega_{\text{eff}})$. On the other hand, if $\delta>\Omega_{\text{eff}}$, only a fraction $\Omega_{\text{eff}}^2/(\Omega_{\text{eff}}^2+\delta^2)$ is transferred into the other magnetic state. In our system, typical values of the effective Rabi frequency are of the order of tens of MHz. This is of the same order as the magnetic splitting of 50 MHz estimated above, and significant Raman transitions into different magnetic levels are expected. Note that according to Eq. (22) the magnetic level splitting at the trap center can be increased, and thus the Raman effect reduced, by increasing the offset magnetic field, e.g., with the help of additional current-carrying wires on the chip. However, this comes at the cost of smaller trap depths and oscillation frequencies, see Eq. (20). We therefore conclude that magnetic trapping in the presence of the evanescent light fields from the disk would be difficult to achieve in practice, even in the direction along the perimeter of the disk where no optical dipole forces exist.

IV. ATOM TRAPPING

A. Trapping potential

The discussion in the previous section shows that magnetic and van der Waals forces will in general be too weak to form trapping potentials for atoms near the microdisk surface in the presence of the detection light field. In the following, we will therefore investigate atom trapping using *two* light fields: a blue-detuned detection light, which also provides a repulsive potential to keep atoms away from the surface against the atom-surface force, and an additional red-detuned field to provide a long-range attractive potential that will keep the atoms close enough to the interaction region with the detection light.

Two objectives must be achieved by the choice of trap parameters. (i) The trap center must be within 50–200 nm of the disk surface to allow for atom detection with sufficient signal-to-noise ratio, e.g., $S>10$. (ii) The depth has to be large enough to keep the atom trapped for the detection time, taking into account any heating effects.

In Fig. 3, we show sample potentials for a rubidium atom coupled to the $(l=167,q=1)$ blue-detuned mode and the $(l=163,q=1)$ red-detuned mode of a 30 μm microdisk. The light intensities create a trapping potential of about 1.9 mK at a distance of 115 nm from the surface. The surface potential reduces the potential depth by lowering the potential barrier toward the disk surface and also slightly shifts the center position.

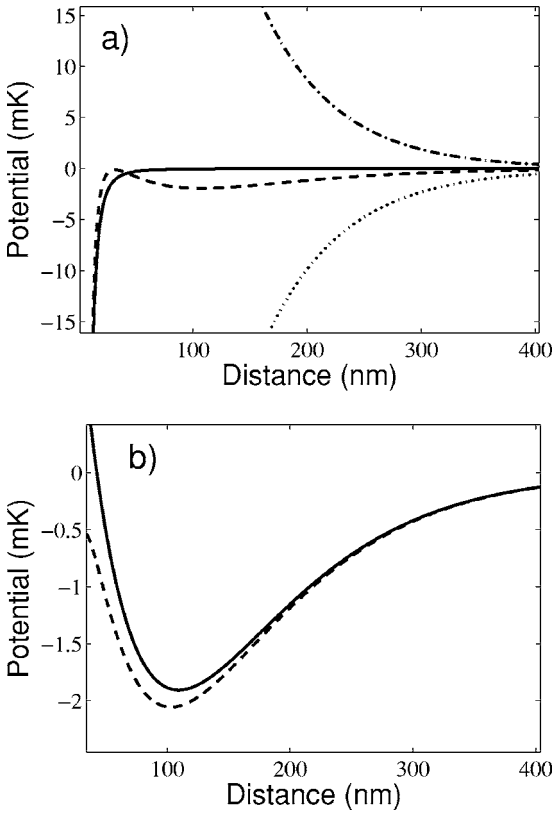

FIG. 3. The radial potential near the surface of a 30 μm disk. (a) Potential formed by blue-detuned light (dash-dotted line) and red-detuned light (dotted), surface potential (solid) and sum potential (dashed). (b) The sum of the optical potentials (solid) and the sum of the optical potentials and the surface potential (dashed). In this example, the number of blue-detuned cavity photons is $N_b=2.4\times10^5$, and the number of red-detuned photons is $N_r=3.68\times10^5$.

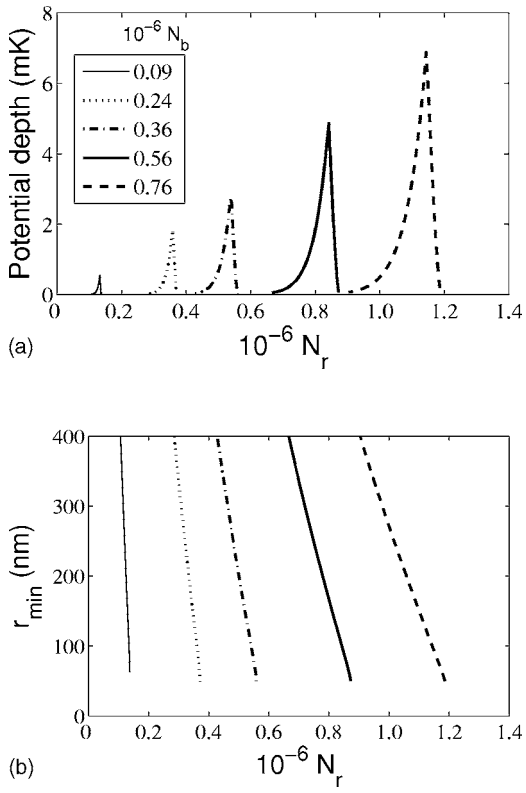

FIG. 4. (a) Potential depth and (b) position of the trap minimum vs photon number N_r in the red-detuned mode for different values of N_b, the photon number in the blue-detuned mode. The disk diameter is 30 μm.

Before investigating trap optimization numerically in more detail, we will first discuss a few trap properties in a simple analytic approximation. For this, we approximate the evanescent fields by decaying exponentials, i.e., the blue-detuned potential is written as $V_b(r)=V_{b0}e^{-\alpha_b r}$, where $V_{b0}>0$ and r is the distance from the disk surface, and the red-detuned potential is $V_r(r)=V_{r0}e^{-\alpha_r r}$ with $V_{r0}<0$. The decay coefficients $\alpha_{r,b}$ are given in Table I. A minimum of the combined effective potential is formed when the two corresponding forces cancel. Close to the surface the repulsive force must dominate, that is, $\alpha_b V_{b0}>\alpha_r|V_{r0}|$. The minimum is formed at a distance

$$r_{\min}=\frac{1}{\alpha_b-\alpha_r}\log\frac{V_{b0}\alpha_b}{|V_{r0}|\alpha_r}. \tag{24}$$

The potential at this point is given by

$$V(r_{\min})=-V_{b0}e^{-\alpha r_{\min}}\frac{\alpha_b-\alpha_r}{\alpha_r}, \tag{25}$$

which is typically a few percent of the single-frequency potentials. At the minimum, the potential is quadratic with oscillator frequency

$$\omega_{\rm ho}=\sqrt{\alpha_r\alpha_b V(r_{\min})/m}. \tag{26}$$

Note that the potential is very sensitive to the field intensities: if $|V_{r0}|$ changes by δV_{r0}, the corresponding change in the location of the minimum is

$$\delta r_{\min}=\frac{1}{\alpha_b-\alpha_r}\frac{\delta V_{r0}}{|V_{r0}|}. \tag{27}$$

Because of the small difference between the two coefficients α_b and α_r (see Table I), a small change of the magnitude of the potentials will significantly shift the minimum of the combined potential. Due to this high sensitivity to light intensities, a more accurate form of the optical potential must be examined. For the following calculations, three effects are taken into account:

(i) The exact form of the potential is given by Hankel functions [13] instead of exponentials. Furthermore, atomic saturation effects render the optical potential nonlinear in the light intensities, see Eq. (9).

(ii) The combined potential formed by the two modes is slightly different than the sum of the two potentials from each mode alone, cf. the discussion in Sec. III A.

(iii) While the van der Waals potential is significantly smaller than the potential of each light field individually, it may still have an appreciable effect on the sum potential, as the red- and blue-detuned fields largely cancel each other.

The sensitivity of the optical trap to the intensity of the red-detuned light for a fixed intensity of the other mode, as motivated by Eq. (27), is discussed in Fig. 4. The figure

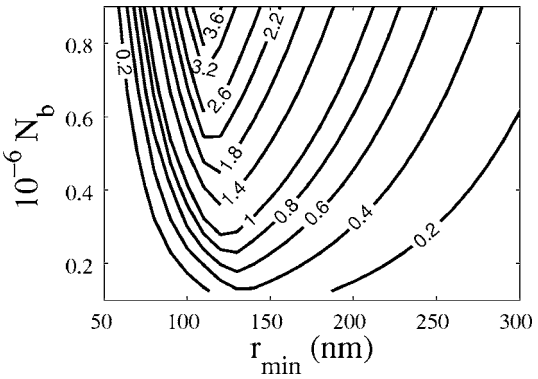

FIG. 5. Contour plot of the potential depth (in mK) vs position of the trap minimum $r_{\min}$ and photon number N_b in the blue-detuned mode for a disk diameter of 15 μm.

shows the potential depth, i.e., the energy difference between the minimum of the potential and the maximum towards the disk surface as seen in Fig. 3, and the position of its minimum versus the red-detuned photon number N_r. For too small values of N_r, no trapping potential exists and atoms are either attracted to the disk surface by the atom-surface interaction or repelled toward infinity by the blue-detuned light. For too large values of N_r, the attractive optical force always dominates over the repulsive force and all atoms are attracted to the disk surface. Trapping occurs for a small range of intermediate red-detuned photon numbers. The maximum potential depth for the chosen parameters is $\sim$7 mK and the corresponding center of the trap is at $\sim$120 nm.

We summarize the dependence of the potential depth on the intensity of the detection (blue-detuned) light N_b and on the distance $r_{\min}$ for disk sizes 15 and 30 μm in Figs. 5 and 6, respectively. For each pair of values N_b and $r_{\min}$ in these figures, the intensity of the red-detuned light N_r is chosen to yield a trap center at this position $r_{\min}$.

Note that by increasing the intensity of *both* light fields, arbitrarily deep optical potentials can be created in principle. However, this will also change the detection efficiency and increase the backaction on the atom itself, as will be discussed later.

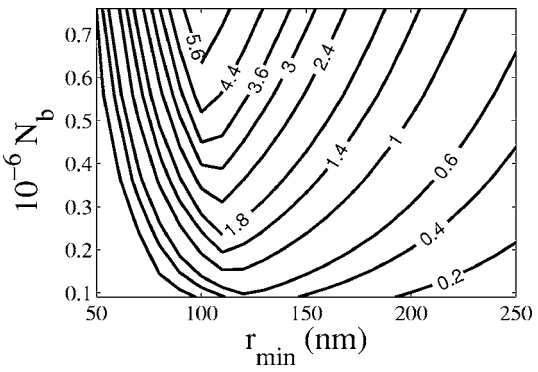

FIG. 6. Contour plot of the potential depth (in mK) vs position of the trap minimum $r_{\min}$ and photon number N_b in the blue-detuned mode for a disk diameter of 30 μm.

B. 3D trapping

So far, we have only discussed trapping in the radial direction from the disk surface. However, we would like to ensure full three-dimensional trapping. First, this would enable us to use an atom again after detection, and, furthermore, tight 3D confinement would reduce atomic heating as discussed in Sec. IV C.

The optical potential that is formed by the evanescent field of the WGMs in the disk also depends on the z coordinate along the height of the disk. The field intensity along this axis can be approximated by $V(z) \approx V(H/2)\cos^2[\pi(1-2z/H)/2]$, where H is the height of the disk [22]. Thus, the intensity vanishes at the edges $z=0$ and $z=H$ of the disk. In the center, at $z=H/2$, a potential minimum is formed with harmonic-oscillator frequency

$$\omega_{z,\mathrm{ho}} = \frac{\pi}{H}\sqrt{|V_{\max}|/m}. \tag{28}$$

This frequency is typically a few kHz, which is an order of magnitude smaller than the radial trapping frequency.

Confinement in the angular direction may be achieved if we create a red-detuned standing wave by inputting red-detuned light from the two sides of the linear waveguide equally to create a superposition of clockwise and counterclockwise propagation around the disk. In this case, the red-detuned and blue-detuned light potential will be given by

$$V_{\mathrm{red}}(x,y,z) = V_{\mathrm{red}}(0,0,H/2)e^{-\alpha_r x}\cos^2[\pi(z-H/2)/H] \times \cos^2(l_r y/R), \tag{29}$$

$$V_{\mathrm{blue}}(x,y,z) = V_{\mathrm{blue}}(0,0,H/2)e^{-\alpha_b x}\cos^2[\pi(z-H/2)/H], \tag{30}$$

where l_r is the winding number of the red-detuned WGM and $R=D/2$ is the microdisk radius. The harmonic-oscillator frequency of the trapping potential in the y direction is then

$$\omega_{y,\mathrm{ho}} = \frac{l_r}{R}\sqrt{|V_{\mathrm{red}}^{\max}|/m}. \tag{31}$$

where V_{red}^{max} is the red-detuned potential at the center of the trap.

Finally, in order to ensure trapping, we need to ensure that the tunneling probability to the disk is negligible. For typical values of barrier height of 1–2 mK and barrier width of 30–60 nm, we expect that no significant tunneling will occur in a time of less than a few seconds. In order to keep these values of barrier height and width, the trapping distance of the atom from the surface must be larger then $\sim$80 nm.

C. Heating of a trapped atom by spontaneous emission

Interaction of the atom with the trapping and detection light fields will in general also induce heating of the atom. Two heating mechanisms can be distinguished: fluctuations of the dipole forces due to, for example, mechanical vibrations or laser instability, and recoil heating after spontaneous-emission events [23]. Here we will focus on the latter heating mechanism.

In a shallow potential well, each spontaneously emitted photon will on average add one photon recoil energy $E_r = \hbar^2 k^2/(2m)$ to the kinetic energy of the photon, where k is the wave vector of the photon. Thus, if we define

$$M = 2\Gamma \tau \rho_{11} \tag{32}$$

as the number of spontaneous-emission events during the atom detection time τ, the total heating is given by ME_r. We therefore require potential depths $V > ME_r$ in order to hold an initially ultracold atom in the trapping potential during the interaction with the light fields.

In a steep potential well, on the other hand, atom trapping is aided by the Lamb-Dicke effect: an atom in the oscillatory ground state is much more likely to return to the same state after a spontaneous emission than to be excited to a higher oscillation state. In the following, we will derive an expression for the probability of the atom to remain in the ground state of motion during the detection time.

Let us assume that the potential may be approximated as a harmonic potential $V = \frac{1}{2} m(\omega_x^2 x^2 + \omega_y^2 y^2 + \omega_z^2 z^2)$ with ground-state sizes x_0, y_0, z_0 in the three directions, respectively. The probability that an atom in the harmonic ground state $|\psi_0\rangle$ returns into the same state after the emission of a photon with wave vector $\mathbf{k}$ is given by

$$P_0(\mathbf{k}) = |\langle \psi_0 | e^{i(k_x x + k_y y + k_z z)} | \psi_0 \rangle|^2. \tag{33}$$

Averaging over all possible directions of $\mathbf{k}$ yields

$$P_0 = \frac{\sqrt{\pi}}{2} \frac{\mathrm{erf}(\mathrm{k} r_0)}{k r_0}, \tag{34}$$

where

$$r_0 = \sqrt{x_0^2 + y_0^2 + z_0^2} = \sqrt{\frac{\hbar}{2m}\left(\frac{1}{\omega_x} + \frac{1}{\omega_y} + \frac{1}{\omega_z}\right)}. \tag{35}$$

For $k r_0 \ll 1$, this may be approximated by

$$P_0 \approx 1 - \frac{k^2 r_0^2}{3} = 1 - \frac{\hbar k^2}{6m}\left(\frac{1}{\omega_x} + \frac{1}{\omega_y} + \frac{1}{\omega_z}\right). \tag{36}$$

After M spontaneous emissions, the probability of staying in the ground state is P_0^M and thus the probability of scattering into excited states of motion is given by

$$P_{\mathrm{other}}(\tau) = 1 - P_0^M \approx 2\Gamma \rho_{11} \tau \frac{\hbar k^2}{6m}\left(\frac{1}{\omega_x} + \frac{1}{\omega_y} + \frac{1}{\omega_z}\right). \tag{37}$$

If this probability is much smaller than unity, the atom will stay in the ground state during the detection process with high probability.

D. Trapping stability

Bichromatic atom trapping has already been used in several applications, beginning from the work of Ovchinnikov *et al.* [24], where two colors with different evanescent decay lengths have been proposed in order to trap atoms at a distance λ from a prism surface. The two-color scheme has been considered also for a dielectric microsphere, a free-standing channel waveguide, and an integrated optical waveguide [23,25–28]. The backaction of an atom on the bichromatic light field in the strong-coupling regime was considered for atom trapping and cooling in Ref. [29].

The main disadvantage of bichromatic trapping, as was pointed out by Burke *et al.* [27], is that trapping is achieved by a fine balance between two optical fields, such that even a small intensity fluctuation may drastically change the trapping conditions or even destroy the trap. Such spatial intensity fluctuations usually exist in real waveguides due to imperfections that generate backscatterred waves that interfere with the main light wave. It was shown [27] that even a backscattered wave, whose intensity is only 0.001 of the propagating mode intensity, may decrease the potential depth by a half and consequently destroy the trap.

Here we analyze the intensity spatial fluctuations due to backscattering in the microdisk structure. We show that backscattering may be decreased to a level where such fluctuations will not severely change the trapping conditions. This is achievable by increasing the coupling rate between the linear waveguide and the microdisk. This increase may affect the detection signal-to-noise ratio, and consequently the integration time will need to be increased.

As was described in [13], the linear coupling between the two counterpropagating modes is described by a complex coefficient ϵ, which is related to the intrinsic loss rate of the disk κ_{int} due to imperfections. The total loss rate of the disk κ is a sum of this intrinsic loss and the loss κ_T due to waveguide-disk coupling [13], such that $\kappa_{\mathrm{int}} = \kappa - \kappa_T$. In this model, the mode amplitudes are given by complex numbers α_+ and α_-, respectively, such that $|\alpha_\pm|^2 = N_\pm$ are the numbers of photons in the two modes. If the disk is pumped with rate η, then the steady-state values of $\alpha_\pm$ are given by

$$\alpha_- = (\epsilon/\kappa)\alpha_+, \tag{38}$$

$$\alpha_+ = \frac{\eta}{\kappa(1 + \epsilon^2/\kappa^2)} \tag{39}$$

so that the backscattered to propagating ratio is given by

$$(I_-/I_+)^{1/2} = \frac{\epsilon}{\kappa - \kappa_T}\frac{\kappa - \kappa_T}{\kappa} = \frac{\epsilon}{\kappa_{\mathrm{int}}}\left(1 - \frac{\kappa_T}{\kappa}\right). \tag{40}$$

With high-quality microdisk resonators, $\epsilon/\kappa_{\mathrm{int}} \approx 1$ can be achieved [3]. Using this value we find that if we wish to keep the trap depth fluctuations smaller than $\pm 2\%$ [meaning $(I_-/I_+)^{1/2} < 1\%$ [30]], we require $\kappa_T/\kappa > 0.99$. This value may be achieved by decreasing the gap between waveguide and microdisk to ~ 0.46 μm in both disks of diameters $D = 30$ and 15 μm, with corresponding Q values of $Q \approx 1.7 \times 10^6$ and $Q = 0.9 \times 10^6$, respectively. In this case, $I_-/I_+ = 10^{-4}$, i.e., an order of magnitude better than that considered by Burke *et al.*, which leads to acceptable trapping instabilities. Thus we believe the concerns of Burke *et al.* described earlier, regarding the destruction of the trap due to backscattered light, are not warranted for state-of-the-art microdisks.

V. DETECTION OF TRAPPED ATOMS

Having discussed the principles of atom detection (Sec. II) and trapping (Secs. III and IV), we will now combine all

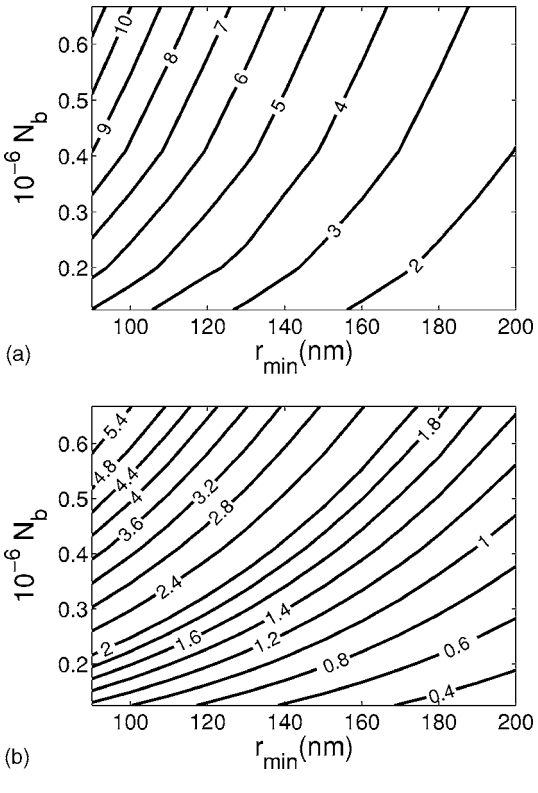

FIG. 7. (a) Signal-to-noise ratio and (b) total (red and blue) scattered photon number vs distance from the disk and blue-detuned photon number for a disk diameter of 15 μm. The integration time is 125 μs.

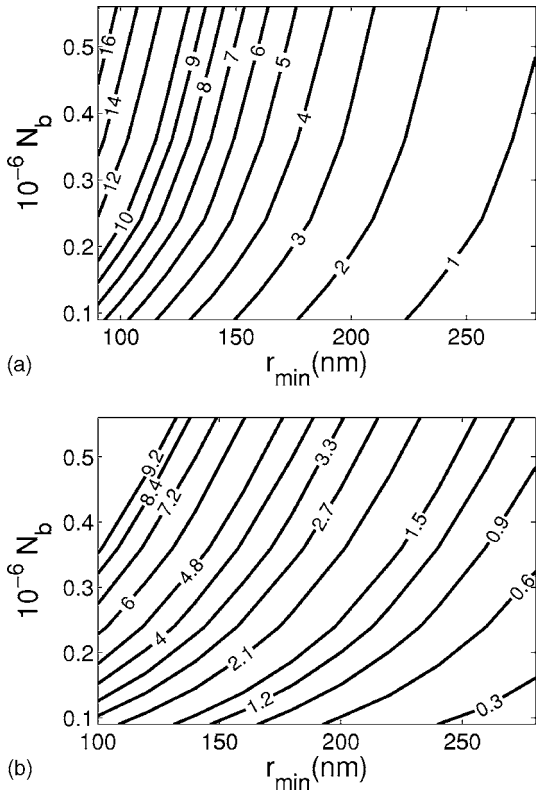

FIG. 8. (a) Signal-to-noise ratio and (b) total scattered photon numbers vs distance from the disk and blue-detuned photon number for a disk diameter of 30 μm. The integration time is 75 μs.

the components and find an optimized set of parameters for efficient simultaneous atom detection and trapping.

We consider the detection and trapping of an atom in a three-level configuration with two light fields. Two disk sizes are investigated: a 30 μm disk using the $(l=167, q=1)$ mode as the blue-detuned detection light and the $(l=163, q=1)$ mode as the red-detuned attractive trapping light, and a 15 μm disk with the $(l=82, q=1)$ mode as the blue-detuned detection light and the $(l=79, q=1)$ mode as the red-detuned attractive trapping light. The optical properties of these modes are given in Table I. For both configurations, we assume surface quality parameters of $\sigma=1$ nm and $L_c=5$ nm, and a gap size of ~ 0.5 μm.

We start our parameter optimization procedure by investigating the single-atom detection efficiency as a function of light intensities. To this end, we show in Figs. 7(a) and 8(a) contour plots of the signal-to-noise ratio S, versus blue-detuned photon number in the disk and versus the position $r_{\min}$ of the trap minimum from the disk surface (this is shown for disk diameters 15 and 30 μm with observation times $\tau = 125$ and 75 μs, respectively). As expected, S increases with increasing light intensity, because of the better photon statistics, and with decreasing atom-disk distance, because of increasing coupling constant $g(\mathbf{x})$.

Next, we calculate the intensity of the red-detuned light required to achieve a trapping potential minimum at given values of $r_{\min}$. From this we obtain the total number of photons M, defined in Eq. (32), spontaneously scattered out of the two light fields by the atom during the detection process. The results show that, in general, larger values of S imply larger numbers of scattered photons M as depicted in Figs. 7(b) and 8(b). However, we note that the parameter dependence of S and M is different, so that optimization is possible.

In Fig. 9, we combine for a $D=15$ μm disk the contour lines for an $S=5$ detection, a heating probability of 5%, Eq. (37), and a tunneling probability of 2%, calculated using the standard expression based on the WKB approximation. The optimal point for atom detection within the parameter region of Fig. 9 is found in the middle of the triangle for $N_b=6 \times 10^5$ and a trap at distance of $r=115$ nm from the disk. In order to achieve atomic trapping at this point we need 2.5×10^5 red-detuned photons in the disk. At this point we obtain $S=8$. The potential depth is 2.6 mK and the harmonic-oscillator frequency is $(\omega_x, \omega_y, \omega_z)=2\pi\times(1.5, 4, 0.14)$ MHz. The ground-state energy of a single atom in this trap is approximately 160 μK and the ground-state dimensions are $(\Delta x, \Delta y, \Delta z)=(15, 6.5, 40)$ nm. The heating probability is 4%. An analysis of the parameter tolerance shows that for these optimized parameters a change of ±2% in either the blue- or red-detuned light intensity will still lead to another point within the triangle of parameters indicated in Fig. 9. A better tolerance could be achieved if light intensities are increased so that the gap between the two lines of signal-to-noise and heating probability in Fig. 9 broadens. However, in this case the potential depth would be decreased, with increased loss of atoms through tunneling to the disk surface.

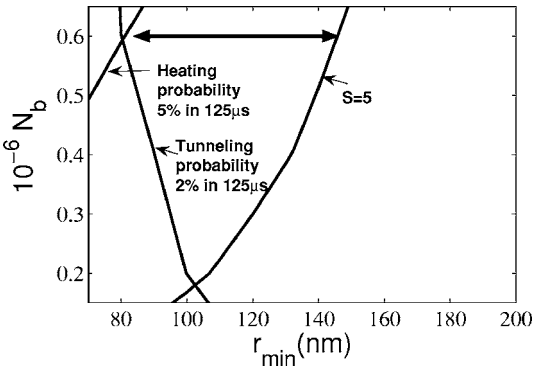

FIG. 9. Performance characteristics of a disk with diameter $D=15$ μm and for a 125 μs integration time, at different blue-detuned photon numbers and atom distances. The area confined by the lines represents $S>5$, heating probability $<5\%$, and tunneling probability of $<2\%$ contains the parameter region where stable atom trapping and detection can be achieved with high confidence. An analysis of the parameter tolerance shows that for these optimized parameters a change of $\pm 2\%$ in either the blue- or red-detuned light intensity will still lead to another point within the triangle. The arrow represents the change in trap position if the intensity of the red- or blue-detuned light is varied by $\pm 2\%$.

The same analysis with the contour lines for $S=5$ and heating probability of 7% for the disk diameter $D=30$ μm gives the optimal point for atom detection within the parameter region of Fig. 10 for $N_b=2.4\times 10^5$ and a trap at distance $r=120$ nm from the disk. In order to achieve atomic trapping at this point we need 3.6×10^5 red-detuned photons in the disk. At this point we obtain $S=7$, the potential depth is 1.6 mK, and the harmonic-oscillator frequency is $(\omega_x,\omega_y,\omega_z)=2\pi\times(0.92,4.2,0.11)$ MHz. The ground-state energy is approximately 126 μK and the ground-state dimensions are $(\Delta x,\Delta y,\Delta z)=(15.9,7.4,46)$ nm. The heating probability is 5.7%. For these optimized parameters, a change of $\pm 2\%$ in either the blue- or red-detuned light intensity will still lead to another point within the area of parameters indicated in Fig. 10, i.e., the blue- or red-detuned intensities may be changed within $\pm 2\%$ while maintaining $S>5$.

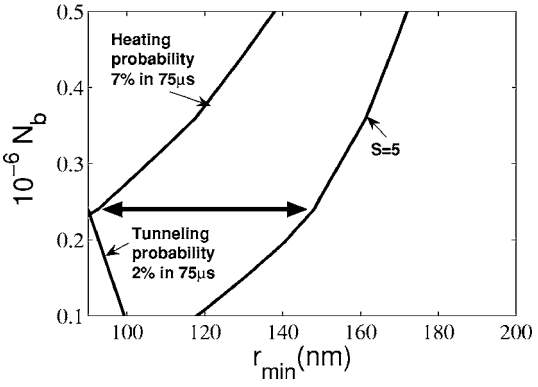

FIG. 10. Performance characteristics of a disk with diameter $D=30$ μm and for a 75 μs integration time, at different blue-detuned photon numbers and atom distances. The area confined by the lines of $S=5$, heating probability 7%, and curve representing tunneling probability of 2% contains the parameter region where stable atom trapping and detection can be achieved with high confidence. The arrow represents the change in trap center position if the intensity of the red- or blue-detuned light is varied by $\pm 2\%$.

VI. EXPERIMENTAL FEASIBILITY AND CONCLUSIONS

We have shown that a single atom can be trapped near the surface of a microdisk resonator such that its presence can be detected with negligible heating. The detection of the atom is done by a blue-detuned WGM of the resonator, while trapping at a fixed position is achieved by a second, red-detuned WGM. The two light fields create a trapping potential at a distance of 100–150 nm from the disk surface. At this distance, the atom-surface attractive interaction (van der Waals force) is much weaker than the light force, while the optical potential is sufficiently strong to create a deep trap for the atom. The atom is then confined in the radial direction and in the z direction (perpendicular to the chip surface). For trapping in the tangential direction we suggest that the red light WGM is coupled to the microdisk from both sides, such that a red-detuned standing wave is formed along the disk perimeter and the atom may be trapped in any of the maxima of the red light.

The use of photonics for atom chips has been discussed recently [31]. Detection of atoms by evanescent fields has been achieved experimentally [32]. Moreover, the use of

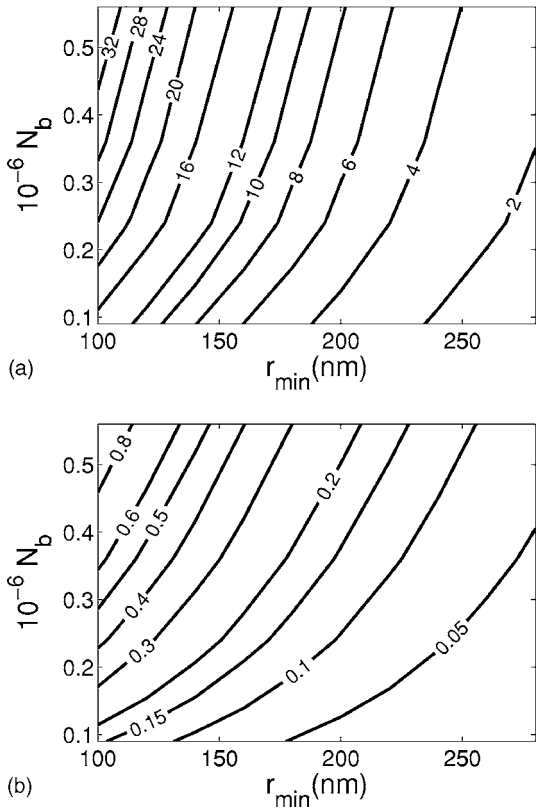

FIG. 11. (a) Signal-to-noise ratio and (b) total scattered photon numbers vs distance from the disk and blue-detuned photon number for disk diameter 30 μm. Integration time is 5 μs, rms roughness $\sigma=0.2$ nm, and gap size ~ 0.7 μm.

bichromatic light for guiding or trapping atoms has also been discussed before [23–29]. The idea of utilizing a two-dimensional microsphere, i.e., a disk or ring with a favorable fabrication feasibility, was put forward by us in a recent paper [13]. In this work, a realistic tolerance analysis combining all the above ideas has been presented. We show that with current fabrication capabilities, a tunable high-Q device may be built to detect single atoms. More specifically, we note that state-of-the-art fabrication has reached a point, where previous concerns regarding the spatial instability of the trapping potential due to light backscatter from imperfections [27] may now be no longer valid. Concerning the required light mode stability, we estimate an acceptable tolerance of $\sim 2\%$. This has been calculated when demanding high stability for the trap parameters as well as atom-light interaction, and is highly dependent on surface roughness and mode coupling. Currently, surface roughness of order 1 nm is achieved by reflow processes where the surface layer is melted and allowed to reform itself with surface tension forces. We have calculated that weak mode coupling and such roughness will enable the above required light intensity accuracy.

Recent experimental works give rise to the possibility of further decreasing surface roughness to below 0.2 nm [33,34]. Applying such roughness to the microdisk, we can decrease the total scattering photon number to below 1 and consequently contemplate the possibility of a true nondestructive measurement (Fig. 11).

The intensity of the input field becomes important also with regard to nonlinear effects. Decreasing the input light intensity can weaken nonlinear mechanisms of instability such as Kerr optical parametric oscillation [35] and radiation pressure-induced mechanical oscillation [36].

Another possibility to achieve trapping during detection is through magnetic trapping. We have shown that magnetic trapping is usually unsuitable for this as optical polarization control is hard to achieve in WGMs and because light-induced Raman transitions will transfer atoms into magnetically untrapped states. Other possibilities such as by use of an attractive electric field may offer more stability, but have their own drawbacks. For example, any metallic electrode near the atom would produce thermally induced EM noise, not to mention absorb and diffract the very sensitive mode of the high-Q resonator. Nevertheless, such options are under investigation and will be analyzed elsewhere.

Further work will also need to address in detail the issue of loading, i.e., how the atoms are brought close to the disk surface. The loading is crucial as it deals with the interplay between the specific atom optics elements such as guides and traps, and the detector responsible for extracting the signal. Here, evanescent disk fields *above* the disk may prove helpful.

Finally, this work described nondestructive detection in the sense of negligible heating during the detection. Future work will need to analyze another harmful mechanism in the form of Raman transitions during the detection between the internal degrees of freedom, i.e., between hyperfine states. It is crucial for quantum technology that detection will not alter the hyperfine state occupancy, as the latter form in most cases the observable of the quantum optics operations.

Let us conclude by stating that we have shown that indeed the road is open for the fabrication of an atom chip in which a microdisk resonator would be integrated. Such an apparatus may offer insight into new experimental regimes, while devices for quantum technology may also be realized.

[1] R. E. Slusher, A. F. J. Levi, U. Mohideen, S. L. McCall, S. J. Pearton, and R. A. Logan, Appl. Phys. Lett. **63**, 1310 (1993); D. Sadot and E. Boimovich, IEEE Commun. Mag. **36**, 50 (1998).

[2] F. Vollmer, D. Braun, A. Libchaber, M. Khoshsima, I. Teraoka, and S. Arnold, Appl. Phys. Lett. **80**, 4057 (2002).

[3] T. J. Kippenberg, S. M. Spillane, D. K. Armani, and K. J. Vahala, Appl. Phys. Lett. **83**, 797 (2003); D. K. Armani, T. J. Kippenberg, S. M. Spillane, and K. J. Vahala, Nature (London) **421**, 925 (2003); V. Zwiller, S. Fälth, J. Persson, W. Seifert, L. Samuelson, and G. Björk, J. Appl. Phys. **93**, 2307 (2003).

[4] M. Pelton, C. Santori, G. S. Solomon, O. Benson, and Y. Yamamoto, Eur. Phys. J. D **18**, 179 (2002); P. Michler, A. Kiraz, C. Becher, L. D. Zhang, E. Hu, A. Imamoglu, W. V. Schoenfeld, and P. M. Petroff, Phys. Status Solidi B **224**, 797 (2001); J. McKeever, J. R. Buck, A. D. Boozer, and H. J. Kimble, e-print quant-ph/0403121.

[5] *The Physics of Quantum Information*, edited by D. Bouwmeester, A. Ekert, and A. Zeilinger (Springer-Verlag, Berlin, 2000).

[6] *Proceedings of the International Workshop on Matter Wave Interferometry*, edited by G. Badurek, H. Rauch, and A. Zeilinger [Physica B & C 151B, No. 1-2 (1988)]; *Atom Interferometry*, edited by P. Berman (Academic Press, San Diego, CA, 1997); A. Peters, K. Y. Chung, and S. Chu, Nature (London) **400**, 849 (1999); T. L. Gustavson, A. Landragin, and M. A. Kasevich, Class. Quantum Grav. **17**, 2385 (2000), and references therein. For atomchip interferometers, see, for example, E. A. Hinds, C. J. Vale, and M. G. Boshier, Phys. Rev. Lett. **86**, 1462 (2001); W. Hänsel, J. Reichel, P. Hommelhoff, and T. W. Hänsch, Phys. Rev. A **64**, 063607 (2001); E. Andersson, T. Calarco, R. Folman, M. Andersson, B. Hessmo, and J. Schmiedmayer, Phys. Rev. Lett. **88**, 100401 (2002).

[7] G. Santarelli *et al.*, Phys. Rev. Lett. **82**, 4619 (1999).

[8] For a review of quantum computing in general, see, for example, Phys. World **11**(3), 33 (1998), special issue on quantum information, edited by M. B. Plenio and V. Vedral; M. B. Plenio and V. Vedral, Contemp. Phys. **39**, 431 (1998); A. M. Steane, Rep. Prog. Phys. **61**, 117 (1998).

[9] R. Folman, P. Krüger, J. Schmiedmayer, J. Denschlag, and C. Henkel, Adv. At., Mol., Opt. Phys. **48**, 263 (2002); J. Reichel, Appl. Phys. B **74**, 469 (2002).

[10] T. Pellizzari, S. A. Gardiner, J. I. Cirac, and P. Zoller, Phys. Rev. Lett. **75**, 3788 (1995); S. J. van Enk, J. I. Cirac, and P. Zoller, Science **279**, 205 (1998); C. J. Hood, M. S. Chapman, T. W. Lynn, and H. J. Kimble, Phys. Rev. Lett. **80**, 4157

(1998); P. W. H. Pinkse, T. Fischer, P. Maunz, and G. Rempe, Nature (London) **404**, 365 (2000).
[11] P. Horak, B. G. Klappauf, A. Haase, R. Folman, J. Schmiedmayer, P. Domokos, and E. A. Hinds, Phys. Rev. A **67**, 043806 (2003).
[12] B. Lev, K. Srinivasan, P. Barclay, O. Painter, and H. Mabuchi, Nanotechnology **15**, S556 (2004).
[13] M. Rosenblit, P. Horak, S. Helsby, and R. Folman, Phys. Rev. A **70**, 053808 (2004).
[14] V. Lefevre-Seguin and S. Haroche, Mater. Sci. Eng., B **48**, 53 (1997).
[15] W. von Klitzing, R. Long, V. S. Ilchenko, J. Hare, and V. Lefevre-Seguin, New J. Phys. **3**, 14 (2001).
[16] D. W. Vernooy, V. S. Ilchenko, H. Mabuchi, E. W. Streed, and H. J. Kimble, Opt. Lett. **23**, 247 (1998); D. W. Vernooy, A. Furusawa, N. P. Georgiades, V. S. Ilchenko, and H. J. Kimble, Phys. Rev. A **57**, R2293 (1998).
[17] C. J. Vale, B. V. Hall, D. C. Lau, M. P. A. Jones, J. A. Retter, and E. A. Hinds, Europhys. News **33** No. 6 (2002).
[18] M. Hammer, K. R. Hiremath, and R. Stoffer, in *Microresonators as Building Blocks for VLSI Photonics*, edited by F. Michelotti, A. Driessen, and M. Bertolotti, AIP Conf. Proc. No. 709 (AIP, Melville, NY, 2004).
[19] D. R. Rowland and J. D. Love, IEE Proc.-J: Optoelectron. **140**, 177 (1993).
[20] S.-T. Wu and C. Eberlein, Proc. R. Soc. London, Ser. A **455**, 2487 (1999).
[21] S.-T. Wu and C. Eberlein, Proc. R. Soc. London, Ser. A **456**, 1931 (2000).
[22] O. Aoyama and N. Yamauchi, Trans. Inst. Electr. Eng. Jpn., Part C **122C**, 1721 (2002).
[23] D. W. Vernooy and H. J. Kimble, Phys. Rev. A **55**, 1239 (1997).
[24] Y. B. Ovchinnikov, S. V. Shulga, and V. I. Balykin, J. Phys. B **24**, 3173 (1991).
[25] H. Mabuchi and H. J. Kimble, Opt. Lett. **19**, 749 (1994).
[26] A. H. Barnett, S. P. Smith, M. Olshanii, K. S. Johnson, A. W. Adams, and M. Prentiss, Phys. Rev. A **61**, 023608 (2000).
[27] J. P. Burke, Jr., S.-T. Chu, G. W. Bryant, C. J. Williams, and P. S. Julienne, Phys. Rev. A **65**, 043411 (2002).
[28] F. Le Kien, V. I. Balykin, and K. Hakuta, Phys. Rev. A **70**, 063403 (2004).
[29] P. Domokos and H. Ritsch, Europhys. Lett. **54**, 306 (2001).
[30] The intensity change due to the additional counterpropagating mode is given by $I_+ \rightarrow I_+[1+I_-/I_++2(I/I_+)^{1/2}\cos(\varphi)]$, where φ is an arbitrary relative phase. If the counterpropagating mode intensity is 0.01% of the propagating mode, then the sum intensity is changed by 2%.
[31] G. Birkl, F. B. G. Buchkremer, R. Dumke, and W. Ertmer, Opt. Commun. **191**, 67 (2001).
[32] R. A. Cornelussen, A. H. van Amerongen, B. T. Wolschrijn, R. J. C. Spreeuw, and H. B. van Linden van den Heuvell, Eur. Phys. J. D **21**, 347 (2002).
[33] K. K. Lee, D. R. Lim, L. C. Kimerling, J. Shin, and F. Cerrina, Opt. Lett. **26**, 1888 (2001).
[34] R. Rabady and I. Avrutsky, J. Opt. Soc. Am. B **20**, 2174 (2003).
[35] T. J. Kippenberg, S. M. Spillane, and K. J. Vahala, Phys. Rev. Lett. **93**, 083904 (2004).
[36] T. J. Kippenberg, H. Rokhsari, T. Carmon, A. Scherer, and K. J. Vahala, Phys. Rev. Lett. **95**, 033901 (2005).